ELSEVIER

Contents lists available at ScienceDirect

Materials Today Communications

journal homepage: www.elsevier.com/locate/mtcomm





Structural, magnetic, optical, dielectric and electronic properties of R_2NiIrO_6 (R = Pr and Nd): A comprehensive experimental and theoretical investigation

- G. Bhavani ^a, Srijita Chakroborty ^b, Ramesh Mamindla ^c, Manish K. Niranjan ^b,
- K. Ramesh Kumar^a, Sattibabu Bhumireddi^a, B.H. Reddy^d, V. Petkov^e, E.S. Kannan^f,
- T. Durga Rao a,
- ^a Department of Physics, GITAM (Deemed to be University), Visakhapatnam, Andhra Pradesh 530045, India
- b Department of Physics, Indian Institute of Technology Hyderabad, Telangana 502284, India
- ^c Department of Physics, VNR Vignana Jyothi Institute of Technology, Hyderabad, Telangana 500 090, India
- ^d Department of Physics, Government College (Autonomous), Rajamahendravaram, Andhra Pradesh 533103, India
- ^e Department of Physics, Central Michigan University, Mt. Pleasant, MI 48858, United States
- f Department of Physics, BITS Pilani, K K Birla Goa Campus, Zuarinagar, Goa 403 726, India

ARTICLE INFO

Keywords: Double perovskite X-ray diffraction Ferromagnetism Exchange bias Optical band gap Dielectric properties ac conductivity Electronic structure studies

ABSTRACT

Double perovskites are highly promising materials capable of exhibiting a wide variety of phenomena. In this work, we perform a comprehensive experimental and theoretical study of polycrystalline R_2NiIrO_6 (R=Pr and Nd) compounds. Both compounds were synthesised using the solid-state reaction method. Rietveld refinement confirmed a monoclinic structure with the $P2_1/n$ space group for both compounds. The scanning electron images showed the average grain sizes of $0.55~\mu m$ for R=Pr and $0.46~\mu m$ for R=Nd. Fourier transform infrared radiation spectra of the two compounds presented two intense bands at 470 cm⁻¹ and 540 cm⁻¹. The optical measurements revealed that the band gaps of the compounds were in the visible absorption range. The field-cooled magnetisation - field hysteresis measurements indicated exchange bias properties in the synthesised compounds at low temperatures. Both temperature and frequency variation of dielectric constant and loss tangent measurements were conducted. The frequency-dependent ac conductivity measurements indicated that the conductivity increases with the increase of frequency as well as temperature. The Nd_2NiIrO_6 compound showed lower ac conductivities compared to its isostructural Pr_2NiIrO_6 compound. The atomic and electronic structures of Nd_2NiIrO_6 and Pr_2NiIrO_6 were explored using the spin-polarised calculations performed within the DFT+U method. Our results suggested that the inclusion of on-site correlations and repulsions for the d-states of atoms was necessary in order to obtain finite band gaps of Nd_2NiIrO_6 and Pr_2NiIrO_6 systems.

1. Introduction

Double perovskites (DP) with the chemical formula AA'BB'O₆ [1], where A and A' are alkaline or rare earth metals, and B and B' are transition metals, have attracted considerable research interest due to their exceptional and diverse properties [2,3]. These include half-metallicity, multiferroicity, exchange bias, and magneto-dielectricity [4–7]. The structural versatility and the intricate interplay between charge, spin, and lattice dynamics make these materials highly appealing for both fundamental physics studies and practical

applications. A key feature of double perovskites is the flexibility of selecting different elements at the B-site, allowing for tunable properties and a rich spectrum of material behaviours. In most DP materials, magnetic properties primarily depend on whether the B and B' cations contain empty or partially filled d-orbitals, while spontaneous polarization is driven by dipolar interactions between the A and/or A' cations and the oxygen (O^2 -) anions. Furthermore, optical, vibrational, and other fascinating properties are influenced by the octahedral tilting of BO₆ and B'O₆ units, adding another layer of complexity and functionality to these materials [8,9].

E-mail address: drtadisetti@gmail.com (T.D. Rao).

^{*} Corresponding author.

Double perovskites containing 3d and 5d transition metals at the B/B′ sites exhibit a range of intriguing physical properties. The inclusion of 5d elements introduces higher spin-orbit coupling (SOC) and relatively weaker on-site Coulombic repulsion, which fosters unique spin, charge, and orbital interactions compared to 3d elements [10]. In 5d transition metals like iridium (Ir), the spin-orbit coupling (SOC) interaction is of comparable strength to other interactions, such as the on-site Coulomb repulsion (U) and the crystal electric field [11]. Subtle modifications in these interactions can give rise to exotic magnetic and electrical properties.

Ir-based double perovskites with chemical formula A₂NiIrO₆ (A = La, Nd, Eu, Pr, Gd) crystallize in a monoclinic structure with the $P2_1/n$ space group and exhibit complex magnetic behaviours due to magnetic interactions arising from the Ni and Ir magnetic sublattices. Research on Ir-Ni-based double perovskites aims to unravel the interplay of magnetic interactions, explore their potential applications in spintronics, and investigate novel phenomena [12]. Studies on R₂NiIrO₆ (R = La, Pr, Nd) have revealed that reducing the ionic radii of R3+ ions enhances the Néel temperature, emphasising the role of structural factors in determining magnetic behaviour [13]. The structural, magnetic properties of La₂NiIrO₆ (LNIO) have been explored, with particular attention given to its exchange bias (EB) properties [14]. Recently, we examined the structural, magnetic, optical, and electronic properties of Gd₂NiIrO₆ (GNIO) [15]. Notably, both LNIO and GNIO display exchange bias phenomena at low temperatures, attributed to Dzyaloshinskii-Moriya (D-M) interactions, a consequence of their low crystallographic symmetry [14,15]. While the structural and magnetic properties of Pr₂NiIrO₆ (PNIO) and Nd₂NiIrO₆ (NNIO), isostructural to LNIO and GNIO, have been reported previously, their optical and dielectric properties remain unexplored. Furthermore, it is also interesting to conduct theoretical studies on these systems. Therefore, in this work, we synthesised PNIO and NNIO compounds using the solid-state route and carried out comprehensive structural, magnetic, optical, dielectric, and electrical properties using various experimental characterisation probes. We also performed first-principles quantum mechanical studies of structural parameters, electronic structure and optical properties within the framework of density-functional theory (DFT).

2. Experimental details

Polycrystalline double perovskites R₂NiIrO₆ (R = Pr for PNIO and Nd for NNIO) were synthesized using the solid-state method with stoichiometric amounts of Pr₂O₃, Nd₂O₃, NiO, and IrO₂ metal powders. The detailed experimental procedure is available elsewhere [14]. The crystal structure of the compounds was analysed using an X-ray diffractometer (Bruker D8-Discover) with Cu Ka radiation, with a resolution of 0.04° in 20. Microstructural characteristics were examined using a scanning electron microscope (Tescan MIRA, Czech Republic) with a resolution of ≤ 2 nm. Elemental composition and stoichiometry were verified through energy-dispersive X-ray spectroscopy. Fourier transform infrared (FTIR) spectra were recorded using a Bruker Tensor 37 spectrophotometer with a resolution of 0.5 cm⁻¹. Optical band gap measurements were performed in absorbance mode with a UV-VIS-NIR spectrometer (SHIMADZU) with an accuracy of ± 0.3 nm across all regions. Magnetic properties were investigated using a physical property measurement system (PPMS, Quantum Design, USA) equipped with a vibrating sample magnetometer (VSM) with a resolution of 10^{-6} emu. Dielectric and ac conductivity measurements (with accuracy of 0.08 %) were conducted across various frequencies and temperatures (within ± 2 °C accuracy) using the Wayne Kerr ZM2376 LCR meter.

2.1. Theoretical and computational methodology

The density functional theory (DFT) [16] is performed to study the electronic structures of both compounds using the plane wave basis set formalism as implemented in the VASP Package [17]. The combined

nuclei and core electron potentials for each ion are approximated using the projected augmented wave (PAW) potentials [18]. The Kohn-Sham orbitals are expanded in plane wave basis set by using the kinetic energy cutoff of 520 eV. The exchange-correlation (XC) part of the effective potential is treated using the Perdew-Burke-Ernzerhoff (PBE) [19] form of generalized gradient approximation (GGA). The improved bandgaps are also estimated using the SCAN [20] and meta-GGA XC schemes. The on-site correlations for the d orbitals on atoms are included using the GGA+U approach [21]. In the case of Nd and Pr atoms, the localized 4 f states are treated as core states, respectively. In general, the DFT framework does not describe the f-electrons accurately enough due to self-interaction errors. The $(3d^8, 4s^2)$, $(5d^7, 6s^2)$, $(2s^2, 6s^2)$ 2p4) configurations are considered as valence electrons for Ni, Ir and O atoms, respectively. The Brillouin zone is sampled using 8x8x6 Monkhorst-Pack *k*-point mesh in order to perform *k*-space integrations. The atomic coordinates and the unit cell lattice constants are relaxed until the Hellmann-Feynman atomic forces become less than 10 meV/Å. The self-consistency in the calculations is achieved by allowing the total energies to converge down to 10^{-6} eV/cell. The linear optical properties are calculated from the band structure and within the independent-particle approximation [22].

3. Results and discussions

3.1. Structural studies

Fig. 1 presents the room-temperature X-ray diffraction (XRD) patterns of the polycrystalline PNIO and NNIO compounds. The crystal structures of both compounds are analysed using Rietveld refinement with FullProf software. The refinement results confirm that both compounds crystallize in a monoclinic structure with the $P2_1/n$ space group. All observed peaks in the XRD patterns are accurately fitted and correspond to the reflections of the monoclinic structure, with no impurity phases detected. The presence of [011] superstructure reflections at 19.5° for the PNIO compound and at 19.4° for the NNIO compound confirms the formation of rock-salt ordered arrangements of Ni and Ir cations in the BO₆ and B'O₆ octahedra [14]. The similar ionic sizes of the B- and B'-site cations can result in a random arrangement of cations. known as anti-site disorder (ASD), within the materials. The existence of ASD in double perovskites results in B-O-B', B-O-B, and B'-O-B' interactions, which influence the magnetic and other physical properties of the compounds. The degree of order for B-site (Ni/Ir) cations can be calculated using the formula as $S = 2g_B - 1$, where g_B represents the cation's occupancy at its correct site [2]. For a fully ordered B-site, S = 1, whereas S = 0 indicates complete disorder. The refinement results show that S is nearly equal to 1, suggesting minimal disorder in the PNIO and NNIO compounds.

The stability of the crystal structure of double perovskites can be analysed using the Goldschmidt tolerance factor t, defined as

$$t = \frac{1}{\sqrt{2}} \left[\frac{r_A + r_O}{\left(\frac{r_B + r_{B'}}{2}\right) + r_O} \right] \tag{1}$$

Where r_A , r_B , $r_{B'}$, and r_O represent the ion radii at their respective positions. Based on the values of t, the crystal structure can be stabilized in cubic, tetragonal, orthorhombic or monoclinic [23]. The calculated values of t for PNIO and NNIO based on Eq. 1 are 0.868 and 0.862, which supports the stabilization of structures of these compounds in the monoclinic crystal structures. The obtained lattice and structural parameters of PNIO and NNIO compounds are given in Table 1.

The Debye-Scherrer equation is used to calculate the average crystallite sizes D from the main peaks of PNIO and NNIO compounds. The Debye-Scherrer equation is given as

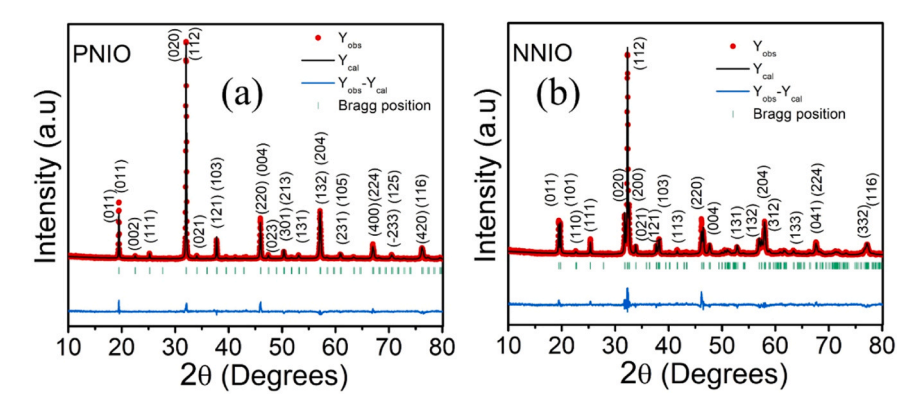


Fig. 1. Room temperature XRD patterns of (a) PNIO and (b) NNIO compound.

Table 1
Lattice parameters, position coordinates, and site occupancies of PNIO and NNIO in the compounds, at 300 K.

Parameters	PNIO		NNIO			
a Å	5.5853 (3)		5.4856 (3)			
b Å	5.5924 (3)		5.6255 (3)			
c Å	7.8935 (4)		7.8023 (4)			
V Å ³	246.557		240.773			
β (°)	90.039 (6)		90.088 (4)	90.088 (4)		
R_{P}	6.39		6.30	6.30		
R _{WP}	8.64		8.07			
χ^2	1.80		1.64			
PNIO	Pr	O_1	O_2	O_3		
x	0.01913	0.02475	0.25450	0.19801		
y	0.53341	0.01229	0.24799	0.30403		
Z	0.74488	0.22433	0.08028	0.53894		
NNIO	Nd	O_1	O_2	O_3		
x	0.02116	0.08806	0.20279	0.20534		
y	0.55072	0.01441	0.27138	0.30886		
Z	0.74904	0.21992	0.06684	0.54753		

$$D = \frac{k\lambda}{\beta \cos\theta} \tag{2}$$

Where, k is the Scherrer constant (0.9), λ is the wavelength of X-rays (1.5405 Å), β is the FWHM (full width at half maximum) in radians, and θ is the Bragg diffraction angle. The calculated D values are 25.3 nm, and 38.8 nm for NNIO and PNIO, respectively. The increase in D is found as the increase in the ionic radius of the A-site ($r_{Nd^{3+}}=0.99$ Å and $r_{Pr^{3+}}=1.013$ Å). [24] Depending on the particular crystal structure and the arrangement of the ions within the lattice, the connection between the ionic radius and crystallite size might change. Even with identical ionic radii, variables such as pressure, temperature and chemical composition during synthesis can have an effect on crystallite size [25].

The lattice strain in the compounds is calculated using the Williamson-Hall method. The Williamson-Hall equation [26,27] is given as

$$\beta \cos \theta = \frac{k\lambda}{D} + 4\varepsilon' \sin \theta \tag{3}$$

Where ε' is the lattice strain, λ is the wavelength of X-rays.

The plot of $\beta cos\theta$, along y-axis and $4sin\theta$ along the x-axis, is a straight line and the slope of which gives the lattice strain of the compounds. The calculated values of lattice strains of PNIO and NNIO compounds are observed to be 1.65×10^{-3} and 1.04×10^{-3} , respectively.

3.2. Microstructural studies

Fig. 2 displays scanning electron micrographs of PNIO and NNIO

compounds. The images show a clear distribution of grains with certain pores, indicating a relatively lower density of the compounds. This reduced density is expected to influence the dielectric and conductivity properties of the materials. The grain size estimation is carried out by calibrating SEM images in ImageJ software. The average grain sizes of PNIO and NNIO compounds are found to be 0.55 μm and 0.46 μm , respectively. The replacement of Pr by Nd at the A-site results in a decrease in the average grain size. The energy dispersive spectra (EDS) confirm the purity of the compounds, with all observed peaks corresponding to the constituent elements of the prepared compounds. EDS analysis further verifies that the stoichiometry of the compounds is retained, with the elemental ratio of Pr/Nd:Ni:Ir:O matching close to the expected ratio 2:1:1:6 in PNIO/NNIO compounds.

3.3. FTIR spectroscopy

The information on molecular structure, functional groups and chemical bonding present in the samples can be observed by using Fourier transform infrared spectroscopy (FTIR). It is also used to investigate the formation of the perovskite structure and to study the vibrational modes present in it. The formation of new peaks and peak shifts are expected, as these correspond to the unique vibrations of functional group interactions induced by the incorporation of various elements at the same or at different lattice sites [28]. Fig. 3 shows the FTIR spectra of the PNIO and NNIO double perovskites. The spectra are similar to the relatively simple spectral patterns of perovskite materials [29,30]. As shown in the figure, the spectra display two distinct and well-defined absorption bands within the 550-400 cm⁻¹ region. The strongest absorption band, with maximum absorption near 540 cm⁻¹, and the second band near 473 cm⁻¹ are observed for both compounds [31]. The strong, high-energy peak at approximately 540.5 cm⁻¹ for both PNIO and NNIO would be attributed to the combined effects of Ir-O and Ni-O stretching vibrations similar to those observed in the literature [32,33]. The band at 424.9 cm⁻¹ would be associated with the deformational modes of the IrO₆/NiO₆ octahedra [34]. This second absorption frequency is also comparable to the second band observed in La₂NiMnO₆ [35]. The FTIR spectra confirm the presence of molecular vibrational bands corresponding to the perovskite oxide structure in the samples.

3.4. Magnetic studies

Fig. 4(a) and (b) show the temperature variation of zero field cooled (ZFC) and field cooled (FC) magnetisation curves under a magnetic field of 1 T from 300 K to 3 K for both PNIO and NNIO compounds. It is observed that the compounds show almost constant magnetisation with the decrease in temperature from 300 K to low temperature, and then they start increasing below 130 K with further decrease in temperature. The ferromagnetic-like magnetic transition temperatures are observed

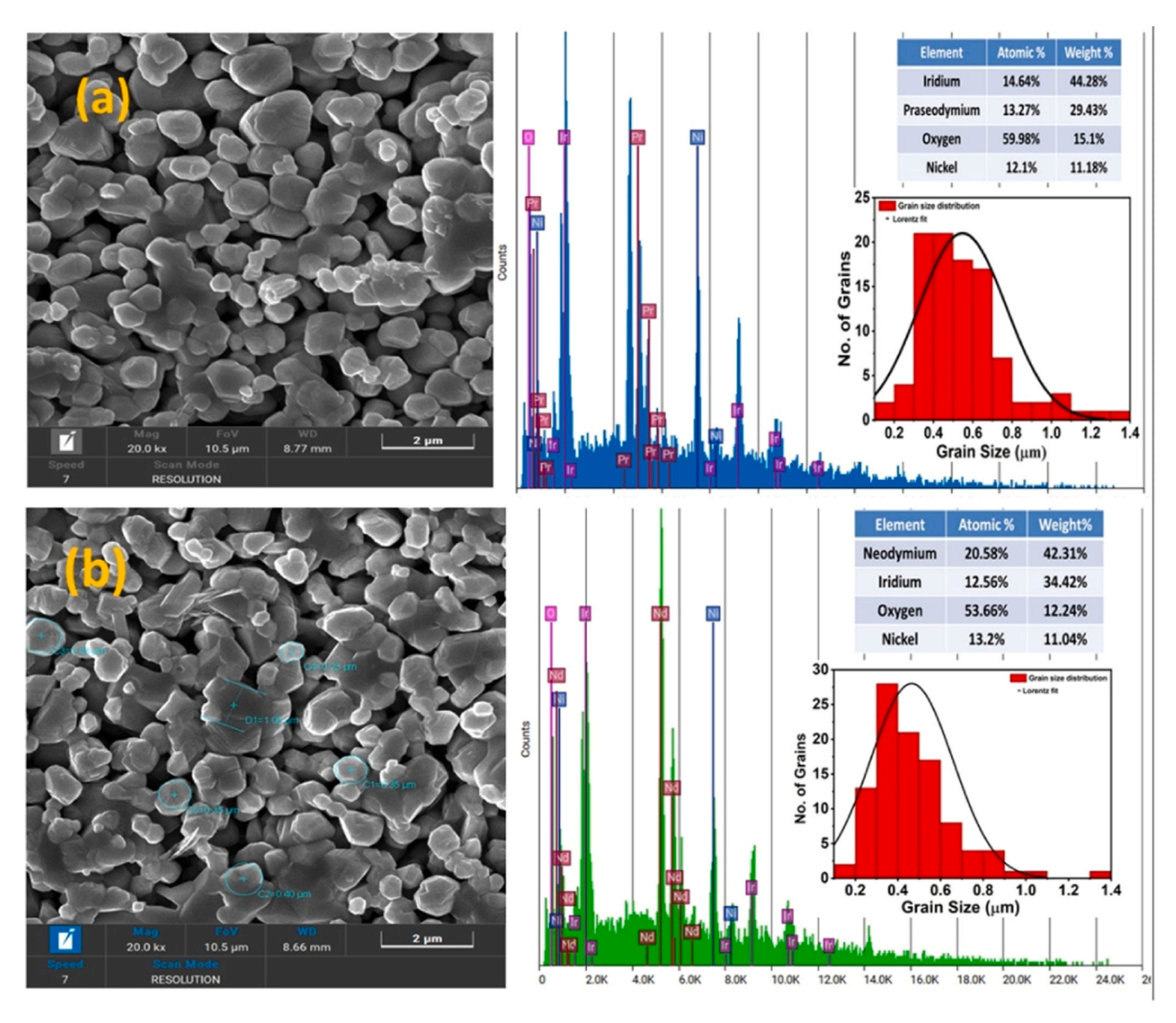
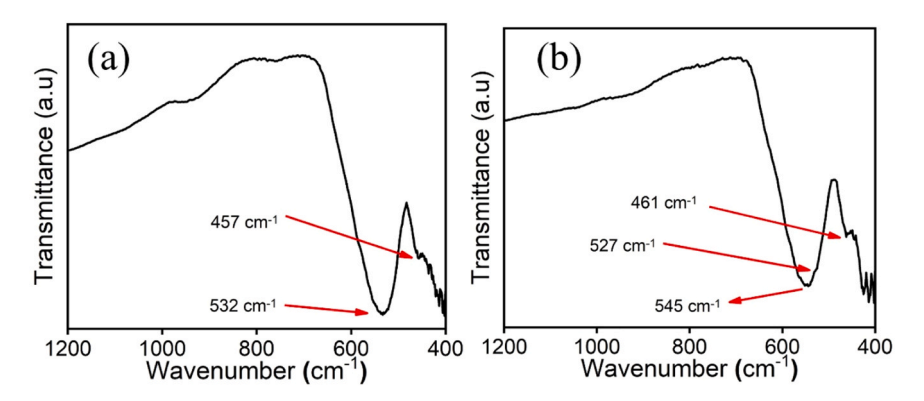


Fig. 2. SEM micrographs of (a) PNIO and (b) NNIO along with EDS spectrum and plot of the distribution of grain sizes.



 $\textbf{Fig. 3.} \ \ \textbf{FTIR} \ \ \textbf{transmittance spectra of (a) PNIO and (b) NNIO double perovskite samples.}$

at 107 K and 117 K for PNIO and NNIO compounds, respectively. The observed ferromagnetic order likely arises from superexchange interactions between Ni²⁺ and Ir⁴⁺ ions mediated by oxygen, consistent with the Goodenough–Kanamori rules [36]. Similar

superexchange-driven ferromagnetic ordering has also been reported in other isostructural double perovskite systems [37]. In addition to these, there would be antiferromagnetic phase due to Ni^{2+} - O^{2-} - Ni^{2+} and Ir^{4+} - O^{2-} - Ir^{4+} exchange interactions. The observed transition

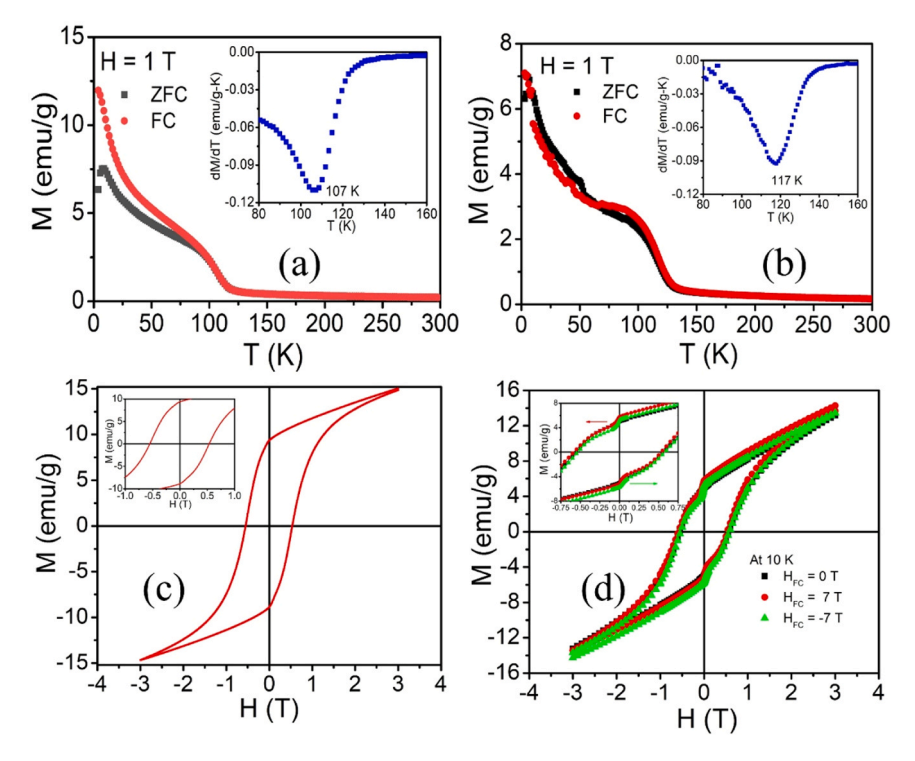


Fig. 4. ZFC FC curves of (a) PNIO and (b) NNIO compounds and insets show the first derivative of FC curve to show the magnetic transitions. The M-H loops of (c) PNIO under the FC field of 7 T, and (d) NNIO compound under the FC fields of 7 T, 0 T and -7 T at 10 K. Insets show the enlarged view of the same M-H plot.

temperatures in PNIO and NNIO compounds are consistent with the literature [38] and can be seen from the first derivative of FC magnetisation curves, as shown in the inset figures for the two compounds. Interestingly, this suggests that a reduction in the ionic radius of the A-site cation results in an increase in the Néel temperature. Further, a low-temperature transition below 10 K is also observed in both compounds. The low temperature transitions observed in PNIO and NNIO compounds may be due to long-range magnetic ordering of rare earth (Pr^{3+} and Nd^{3+}) ions [39,40] or spin glass-like behaviour [41]. In order to know the exact nature of the transition, ac susceptibility measurements and neutron diffraction studies to be conducted.

It is observed that both ZFC and FC curves start to bifurcate below 130 K. The bifurcation in ZFC and FC curves is also called thermomagnetic irreversibility, which arises due to the change in magnetic exchange integral paths [42]. At low temperature, thermal energy is insufficient to overcome anisotropy barriers, so spins/domains get pinned differently in ZFC and FC protocols, producing bifurcation.

As the exchange bias properties are observed in the isostructural LNIO and GNIO compounds [14,15], we have investigated the exchange bias properties in these compounds. Fig. 4(c) presents the magnetic hysteresis (M-H) loops for the PNIO compound measured at 10 K, under the field cooling field of 7 T. The M-H loops exhibit ferromagnetic hysteresis loops with remanent magnetisations (M_r) of 9.29 emu/g and coercive fields (H_c) of 545 Oe. Fig. 4(d) presents the magnetic hysteresis (M-H) loops for NNIO compounds measured at 10 K, under the field cooling field of 7 T (red curve). The M_r and H_c of NNIO compound are 5.85 emu/g and 443 Oe, respectively. The magnetisation curves of PNIO and NNIO compounds do not saturate even at the maximum applied field of 3 T, indicating the presence of antiferromagnetic interactions in the compounds. It is interesting to note that exchange bias properties in PNIO and NNIO compounds with exchange bias fields of 375 Oe and 256 Oe, respectively. The coupling between the interfaces of ferromagnetic and antiferromagnetic components leads to the exchange bias effect. In order to test these properties whether intrinsic or not, the M-H hysteresis loops are measured under cooling fields (HFC) of 0 T, and -7 T. When $H_{FC} = 0$ T, the loop is situated symmetrically about the origin. When the $H_{FC}=7$ T, the (red) loop is shifted left, indicating the presence of exchange bias properties in the compound. Further, the (green) loop shifts towards the right when $H_{FC}=-7$ T is applied, verifying the appearance of exchange bias properties in the compound.

3.5. UV-visible spectroscopy

Fig. 5(a) and (b) depict the absorption spectra of the PNIO and NNIO compounds, respectively. The optical band gaps of these compounds are estimated using Tauc's equation given as [43].

$$(\alpha h \nu)^n = A(h \nu - E_g) \tag{4}$$

In this equation, $\alpha,A,h\nu$, and E_g represent the coefficient of absorption, the proportional constant, the photon energy, and the energy gap, respectively.

The insets of Fig. 5(a) and 5(b) present plots of $(ahv)^2$ versus ,hv, where the E_g is determined by drawing and extrapolating the tangent to the most linear section of the plot to its intersection with the abscissa axis. The calculated band gaps are 1.44 eV for the PNIO compound and 1.36 eV for the NNIO compound, confirming their classification as semiconductors [44]. Materials with smaller band gaps are particularly advantageous as they enable the absorption of a broader range of the visible solar spectrum. The band gaps of PNIO (1.44 eV) and NNIO (1.36 eV) suggest their potential for applications in photocatalysis, optoelectronics, solar cells, and sensors [45].

3.6. Dielectric studies

The frequency-dependent dielectric constant (ε_r) and loss tangent ($\tan \delta$) are shown in Fig. 6. According to Maxwell-Wagner's theory of dielectrics, the grain boundaries act as non-conducting layers, whereas grains are conducting for the charge carriers. When the electric field is applied, the charge carriers transfer from high-conducting grains to insulating grain boundaries [46]. As shown in Fig. 6(a) and 6(b) for PNIO and NNIO compounds respectively, ε_r is high, and it decreases with the increase of frequency, showing the inverse relation with the

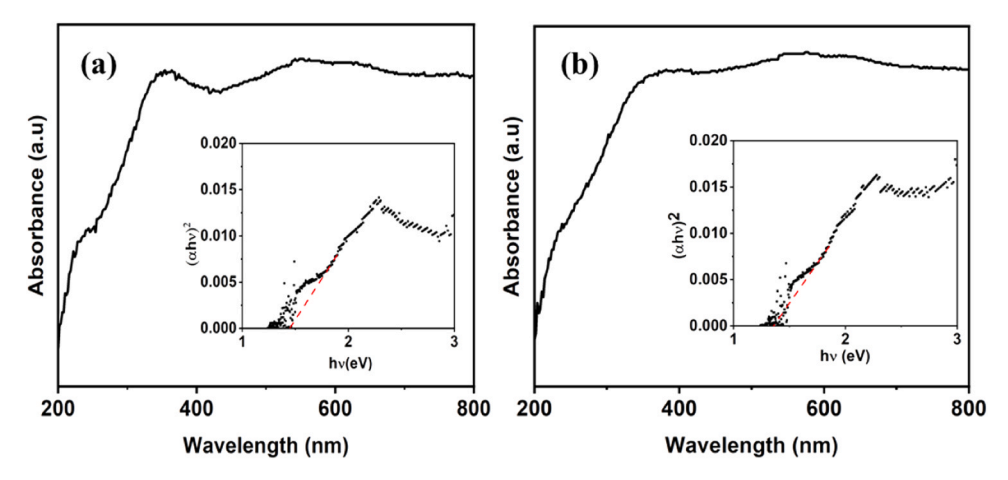


Fig. 5. UV-vis spectrum of (a) PNIO and (b) NNIO compounds. Inset shows the Tauc's plot of the compounds.

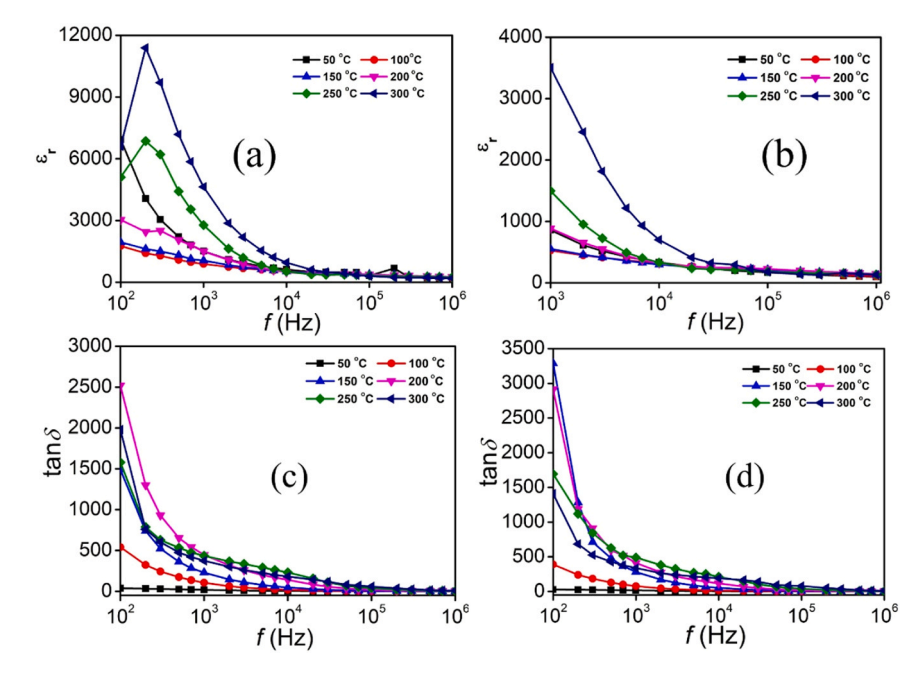


Fig. 6. Frequency variation of ε_r for (a) PNIO, (b) NNIO compounds and frequency variation of $\tan\delta$ for (c) PNIO, and (d) NNIO compounds at different temperatures.

frequency. The high ε_r is ascribed to the contribution of space charge or interfacial, dipolar, ionic and electronic polarizations. As the frequency is increased, the charge carriers are unable to accumulate at the barriers, and the contributions from polarisation mechanisms gradually fade, leading to a decrease in ε_r value. Similar trends can also be observed in the frequency variation of $\tan\delta$ for PNIO and NNIO compounds, as shown in Fig. 6(c) and (d), respectively. The increase in temperature leads to an increase in ε_r and $\tan\delta$ as shown in Fig. 6.

The temperature variations of ε_r and $\tan\delta$ under different frequencies are shown in Fig. 7. It is observed that ε_r slightly increases at low temperatures and increases sharply at high temperatures. At low temperatures, charge carriers such as oxygen vacancies and electrons remain strongly bound to their defect sites, contributing minimally to the dielectric constant. With increasing temperature, these vacancies acquire sufficient energy to become mobile within the lattice, leading to the development of space charge polarization, along with Maxwell–Wagner interfacial and defect dipolar polarizations [41]. Consequently, the dielectric constant increases as the temperature rises. Similar observations have also been reported in the literature [47–50]. At high frequencies, ε_r changes insignificantly due to the gradual diminishment of the contributions to polarisation, except the atomic and

electronic polarisations. The rapidly changing electric field hinders the movement of charge carriers at high frequency inside the dielectric material and hence the decrease in ε_r . The temperature variation of $\tan\delta$ shows a broad peak in the high temperature, which shows similar behaviour as the dielectric constant shows the variation with temperature. At high temperatures, the increase in dc conductivity of the compounds is responsible for the increase in $\tan\delta$. As the temperature increases, the dielectric loss ($\tan\delta$) also rises, exhibiting a broad peak that shifts toward higher temperatures with increasing frequency. This behavior indicates a thermally activated relaxation process in the material, consistent with similar relaxation phenomena reported in the literature [51].

3.7. ac conductivity studies

Fig. 8 shows the variation of ac conductivities of PNIO and NNIO compounds with respect to frequency. The ac conductivity (σ_{ac}) can be calculated by the equation [52]

$$\sigma_{ac} = \varepsilon_r \varepsilon_o \omega \tan \delta \tag{5}$$

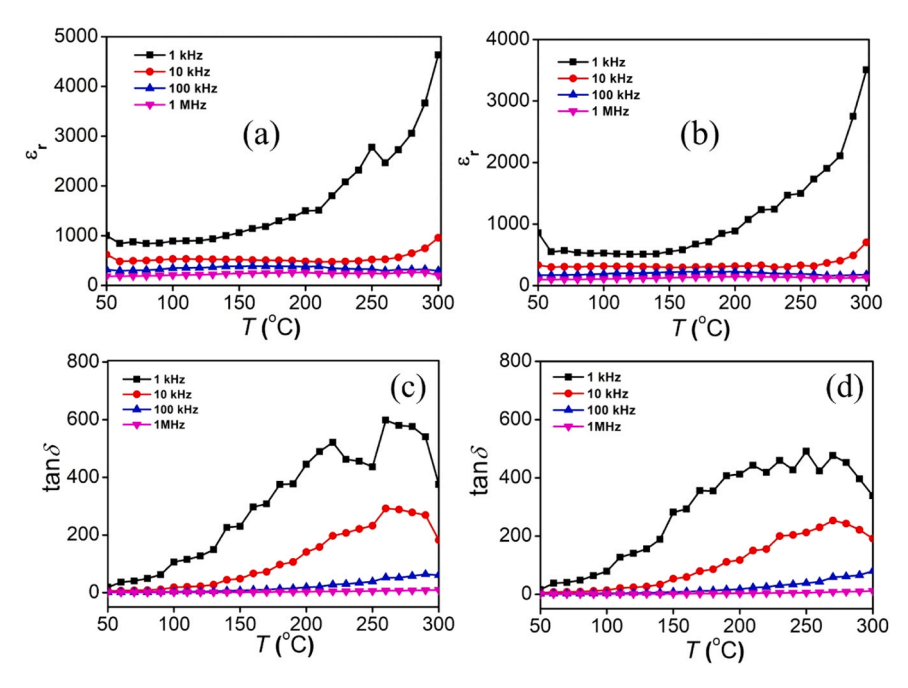


Fig. 7. Temperature variation of ε_r for (a) PNIO, (b) NNIO compounds and temperature variation of $\tan \delta$ for (c) PNIO, (d) NNIO compounds at different frequencies.

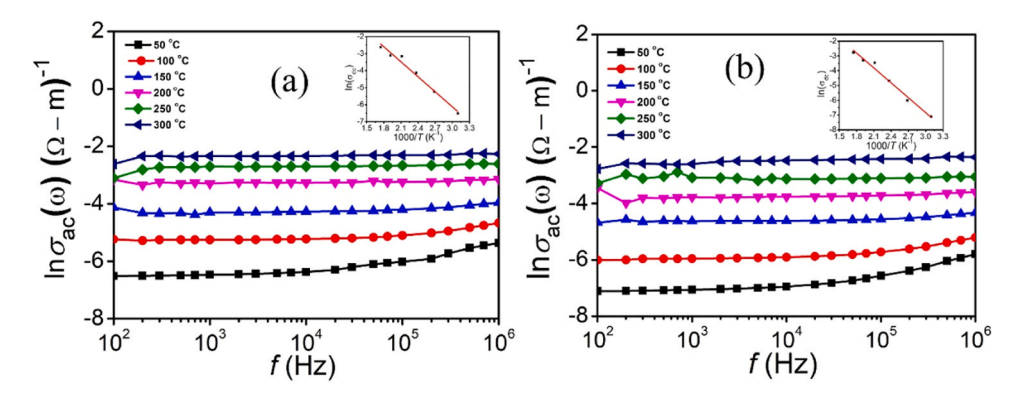


Fig. 8. Frequency variation of ac conductivity of (a) PNIO, and (b) NNIO compounds at different temperatures. Insets in (a) and (b) show the Arrhenius plot of $ln\sigma_{dc}$ versus 1000/T for PNIO and NNIO compounds, respectively.

Where ε_r is the dielectric constant, ε_o is the permittivity of vacuum, $\omega=2\pi f$ and f is the frequency and $\tan\delta$ is the dielectric loss tangent. The ac conductivity is constant at low frequencies and is increasing slightly with the increase in frequency. σ_{ac} exhibits a plateau region where the conductivity is constant up to a certain frequency f_p ; thereafter, it increases. The switchover of conductivity to the frequency dependent region from the frequency independent region specifies the inception of conductivity relaxation in the materials where the charge carriers perform hopping from long-range to short-range at the frequency f_p [53]. The plateau region extends with the increase of temperature, i.e., the value of f_p increases with the increase of temperature. The conductivity corresponding to the low frequency plateau is ascribed to dc conductivity (σ_{dc}) and temperature variation of σ_{dc} follows the Arrhenius equation given as

$$\sigma_{dc} = \sigma_o e^{\frac{-E_a}{kT}}$$

Where E_a is the activation energy and k is Boltzmann's constant. The activation energy can be obtained by finding the slope of the curve drawn between $\ln \sigma_{dc}$ and 1000/T as shown in insets of Fig. 8. The E_a values of 0.25 eV and 0.29 eV are observed for PNIO and NNIO compounds respectively. The low values of E_a could be due to the

hopping of charge carriers between the localized states in the disordered materials [54]. As σ_{dc} increases with the increase in temperature, the conductivity is thermally activated, and the material exhibits a negative temperature coefficient of resistance (NTCR) character. The increase in temperature increases σ_{ac} due to the enhancement of oxygen vacancies, which were formed during the synthesis according to the reaction as suggested by Kröger and Vink [55]

$$O_o \to \frac{1}{2} O_2 \uparrow + V_o^{\bullet \bullet} + 2e^{-1} \tag{6}$$

NNIO compound shows lower σ_{ac} compared to PNIO compound.

3.8. Electronic structure studies

The atomic and electronic structures of NNIO and PNIO are explored using the spin-polarized calculations performed within the DFT+U method. Our results suggest that the inclusion of on-site correlations and repulsions for the d-states of atoms is necessary in order to obtain finite band gaps of NNIO and PNIO systems. The on-site correlations for d-states are taken into account in GGA+U scheme and are absent in the GGA scheme. The systems with strongly correlated d or f electrons are better in much better way by the DFT+U method as compared to

standard GGA XC functionals. The calculations are performed for ferromagnetic (FM) configuration and three different anti-ferromagnetic (AF1 AF2 and AF3) configurations for Ni and Ir atoms with a value of $U=4~\rm eV$ is used for all d-orbitals.

The Fig. 9 shows the relative spin orientation for AF1, AF2 and AF3 configurations. For both compounds, all three AF configurations are found to have comparable energies. In the case of NNIO, the AF1 state is found to be lower by 1.2 meV/atom and 1.19 meV than the AF2 and AF3 states, respectively. For PNIO, the AF2 state is found to be lower by 0.08 meV/atom, 0.87 meV, 0.07 meV/atom than AF2, AF3 and FM states, respectively.

These results suggest that the ground states of these compounds may consist of a more complex spin structure due to competition between different magnetic ordering configurations. Furthermore, nano-regions with FM and different AF orderings and/or competing magnetic spin structures may also exist in the system [56]. Table 2 shows lattice parameters of the optimized unit cells of NNIO and PNIO in AF1, AF2, AF3 and FM states, obtained from spin-polarized calculation with U = 4 eV for the *d*-orbitals of atoms. As can be noticed, the computed lattice parameters are in good agreement with the experimental values and exhibit the trend as expected for GGA XC approximation. The overall computed volumes for both compounds are slightly overestimated $(\sim 1.2 \%)$ as compared to the experiments. This overestimation is expected for the GGA-computed lattice parameters. The GGA bandgap for NNIO is computed to be \sim 1.02 eV and is underestimated in comparison to the experimental values of ~1.36 eV. The underestimation of bandgaps is expected for the GGA XC functionals as much as by $\sim 50~\%$ [22]. The computed bandgap value is also found to vary with the choice of on-site Hubbard parameter U.

Table 3 shows the variation of computed bandgaps with the Hubbard on-site parameter U. The bandgap of NNIO compound computed using SCAN meta-GGA scheme and using $U=4~\rm eV$ is obtained to be 1.56 eV and is in better agreement with the experimental value as compared to GGA values.

The SCAN scheme fulfils all known constraints required for any exact density functional [20], hence is expected to be better than GGA for estimating bandgap. The absolute value of the magnetic moment of each Ir and Ni atom is found to be $\sim 0.7~\mu_B$ and $\sim \! 1.7~\mu_B$, respectively. The bandgap for PNIO compound computed using GGA and U= 4 eV comes out to be $\sim \! 1.05$ eV, which is also underestimated in comparison to the experimental value of $\sim \! 1.44$ eV. The bandgap using SCAN meta-GGA scheme and U= 4 eV is obtained to be 1.65 eV. Table 3 also shows the variation of computed bandgaps of PNIO compound with U. Similar to the NNIO compound, the absolute value of magnetic moments of each Ni and Ir atoms in the PNIO compound are found to be $\sim 1.7~\mu_B$ and $\sim \! 0.7~\mu_B$, respectively.

Fig. 10 shows the total and partial density of states (DOS) and band structure for NNIO in AF1 configuration. The energy scale in Fig. 9(a) is rescaled so that the valence band maximum (VBM) is at 0. The VB

Table 2 Computed lattices parameters and bandgap (eV) of NNIO and PNIO obtained using GGA+U XC functional scheme.

			a(A)	\boldsymbol{b} ($\boldsymbol{\mathring{A}}$)	c (Å)	$V(A^3)$	$\pmb{E_{\rm g}}(\pmb{e}\pmb{V})$
NNIO	Cal.	AF1	5.453	5.790	7.746	244.52	1.01
		AF2	5.435	5.802	7.742	244.08	1.05
		AF3	5.452	5.792	7.735	244.18	1.01
		FM	-	-	-	-	-
	Exp.		5.4856	5.6255	7.8023	240.77	1.36
PNIO	Cal.	AF1	5.512	5.742	7.792	246.61	1.03
		AF2	5.503	5.748	7.801	246.74	1.06
		AF3	5.521	5.748	7.775	246.73	1.04
		FM	5.499	5.761	7.794	246.94	1.11
	Exp.	-	5.5853	5.5924	7.8935	246.56	~1.44

Table 3Computed bandgap (eV) of NNIO and PNIO as function of U parameter.

		2 eV	3 eV	4 eV	5 eV
NNIO	GGA	0.25	0.60	1.01	1.46
	SCAN	0.75	1.13	1.55	2.01
PNIO	GGA	0.29	0.65	1.06	1.50
	SCAN	0.82	1.22	1.64	2.08

extends from ~ -7 eV to VBM at 0 eV. The VB in range -1eV < E < 0 is mainly comprised of Ir-5d states. In range -5 < E < -1eV, the VB is mainly comprised of Ni-3d and O-2p states. The states in range -7 < E < -5eV are mainly comprised of Ir-5d states with smaller contributions of Ni-3d and O-2p states. The conduction band (CB) in the range $1eV < E < 1.5 \ eV$ is primarily contributed by Ir-5d states with smaller contributions of O-2p states. The CB in $5eV < E < 7 \ eV$ is mainly contributed of Nd states. The band structure for NNIO shown in Fig. 10 (b) indicates that the bandgap is likely to be direct.

Fig. 11 shows the total and partial density of states (DOS) and band structure for PNIO in AF2 configuration. As evident, the electronic structure for PNIO is qualitatively similar to that obtained for NNIO. Next, we explore the relative strength and nature of bonding between atoms by analyzing the projected crystal orbital Hamilton populations (COHP) [57].

Fig. 12 shows the COHP as function of energy (E) for Nd-O, Ir-O, Ni-O, Nd-Ir, and Nd-Ni pairs in NNIO. In general, the positive and negative values of COHP (E) can be considered as indicative of bonding and antibonding, respectively. Fig. 12(b) shows the integrated COHP (or ICOHP) values that are obtained by integrating the COHP up to the valence band maximum. The ICOHP magnitudes may also be used to assess the relative strength of the bonding between atoms. As can be seen, the Nd-O and Ir-O bond strengths are significantly higher than that for Ni-O, Nd-Ir and Nd-Ni. The COHPs for PNIO are shown in Fig. 13 and are qualitatively similar to that for NNIO as expected.

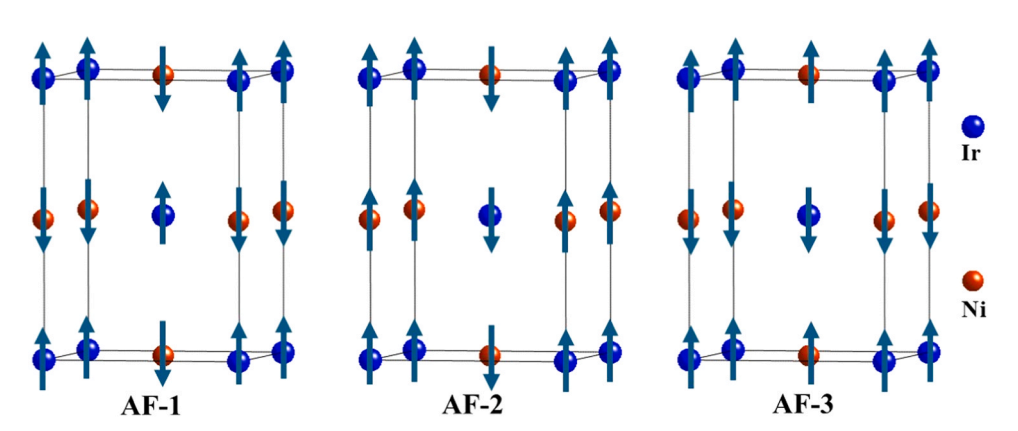


Fig. 9. Antiferromagnetic AF-1, AF-2 and AF-3 configuration states of NNIO and PNIO.

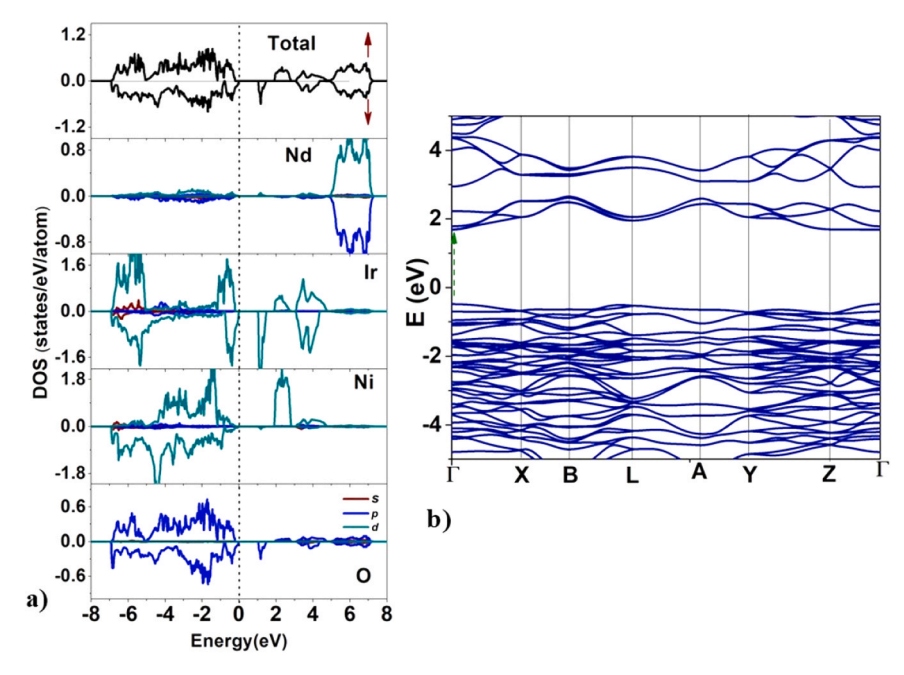


Fig. 10. a) Total and projected density of states and b) band structure for NNIO in AF-1 state. The dotted line in the DOS plot indicates the valence band maximum.

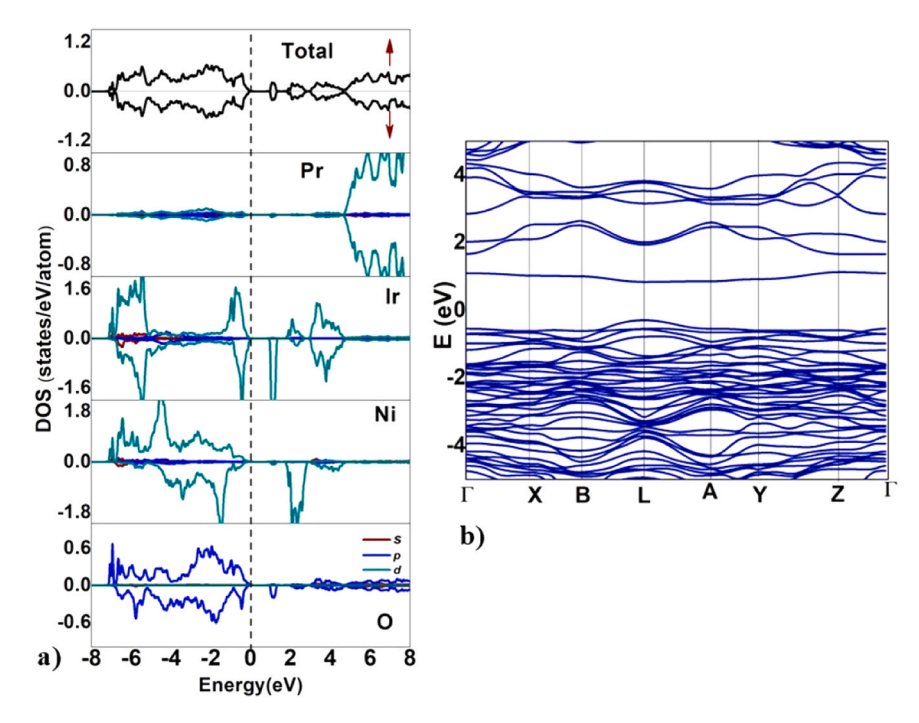


Fig. 11. a) Total and projected density of states and b) band structure for PNIO in AF-2 state. The dotted line in the DOS plot indicates valence band maximum.

We also attempt to estimate the relative charges transfer between bonding atoms by computing the Bader charges (Q_B)) [58]. These charges may also be helpful in the assessment of relative degree of covalent and ionic boding between atoms as well as their oxidation states. The Q_B for Nd, Ir, Ni, and O ions in NNIO are found to be + 2.24, + 1.4, + 1.18 and -1.2 respectively. In case of PNIO, the Q_B for Pr, Ir, Ni, and O ions are + 2.26, + 1.41, + 1.19 and -1.2 respectively. As expected, the Q_B values indicate that the electron charge is transferred from Nd (Pr), Ir, Ni to O atoms. The computed Q_B values are smaller than formal oxidation state of atoms. This suggests that the Ir-O, Ni-O bonding may consist some covalent character as well though the bonding is primarily of ionic type due to charge transfer.

We also compute the optical parameters, such as the absorption coefficient α from the frequency-dependent complex dielectric function $\varepsilon(\omega)=\varepsilon'+i\varepsilon''$ obtained from the electronic band structure [22]. In general, the imaginary part of the dielectric function (ε'') is related to the absorption and its onset indicates the optical band gap. The $(\alpha E)^2$ plots as a function of E for NNIO and PNIO are shown in Fig. 14 and are in qualitative agreement in experiments. It may be noted that the theoretical optical properties discussed in this section reflect only the electronic band structure contribution and thus may differ from the experimental results that may also include contributions from other factors such as sample quality, preparation etc.

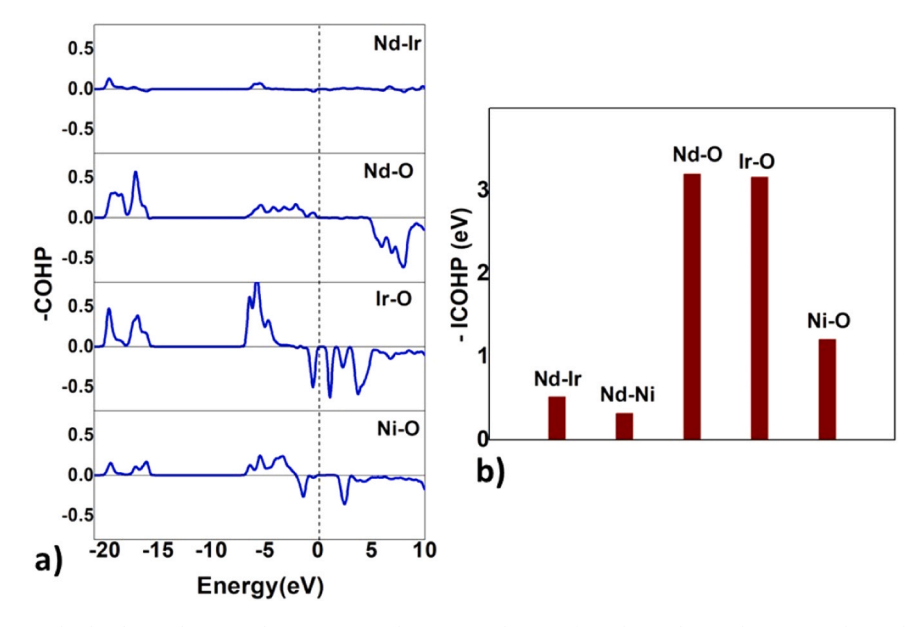


Fig. 12. (a) Crystal orbital Hamilton population (COHP) (b) Integrated COHP for Nd-Ir, Nd-Ni, Nd-O, Ir-O and Ni-O bonds in NNIO.

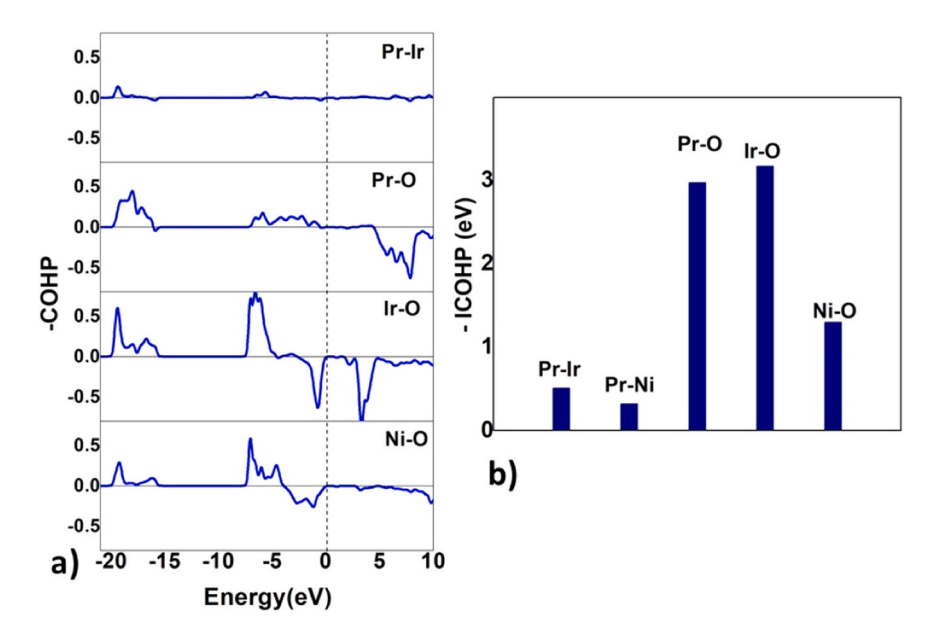


Fig. 13. (a) Crystal orbital Hamilton population (COHP) (b) Integrated COHP for Pr-Ir, or-Ni, Pr-O, Ir-O and Ni-O bonds in PNIO.

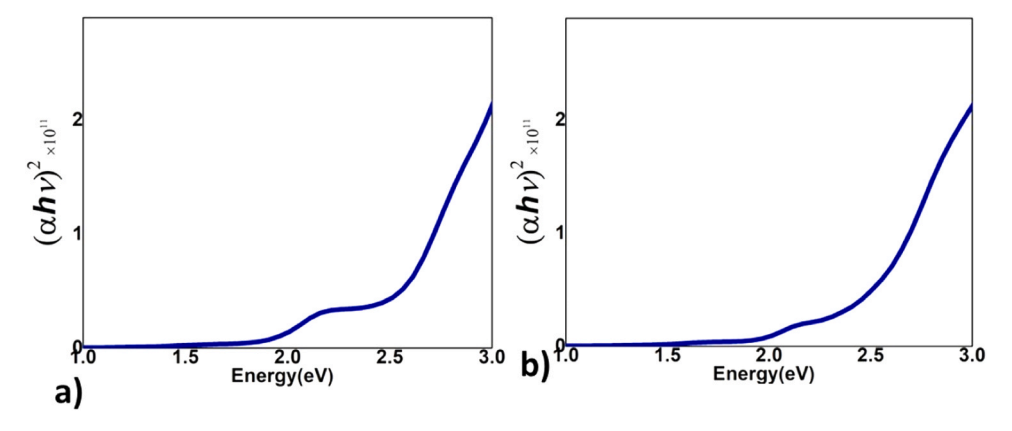


Fig. 14. $(\alpha E)^2$ as a function of energy for a) NNIO and b) PNIO. The α and E are the absorption coefficient and energy, respectively.

4. Summary

Polycrystalline R₂NiIrO₆ (R = Pr and Nd) compounds were synthesised by using the solid-state reaction method. Rietveld refinement showed that compounds stabilised in a monoclinic structure with the $P2_1/n$ space group. The average grain sizes were found to be 0.55 µm for PNIO and 0.46 μm for NNIO compounds. The intense bands observed from 400 cm⁻¹ to 600 cm⁻¹ were corresponding to the Ni/Ir-O vibrational bonds. The optical band gaps of the compounds were observed in the visible absorption range. The exchange bias properties observed at low temperatures are due to the ferromagnetic and antiferromagnetic interactions at the interfaces. The PNIO compound exhibited a higher exchange bias field compared to the NNIO compound. The conductivity of the compounds increased with the increase in frequency as well as temperature. The NNIO compound showed lower ac conductivities compared to its isostructural PNIO compound. First-principles DFT calculations were performed to study the electronic structure of NNIO and PNIO. The theoretical estimates of lattice parameters were found to be in good agreement with the experimental values. The COHP and Bader ionic charge analysis was performed to explore the nature and relative strength of atomic bonding. The optical parameters, such as the absorption coefficient α , were computed from the band structures. We hope that many benchmark results on NNIO and PNIO presented in this work will stimulate further experimental and theoretical research in these and related systems.

CRediT authorship contribution statement

Reddy B. H.: Software, Formal analysis, Data curation, Conceptualization. V. Petkov: Software, Formal analysis, Data curation, Conceptualization. K. Ramesh Kumar: Software, Formal analysis, Data curation, Conceptualization. Sattibabu Bhumireddi: Software, Formal analysis, Data curation, Conceptualization. Ramesh Mamindla: Software, Formal analysis, Data curation, Conceptualization. Manish K Niranjan: Writing – original draft, Software, Data curation, Conceptualization. G. Bhavani: Writing – original draft, Methodology, Data curation, Conceptualization. Srijita Chakroborty: Software, Formal analysis, Data curation, Conceptualization. Rao T Durga: Writing – review & editing, Supervision, Funding acquisition, Conceptualization. Kannan E. S.: Software, Formal analysis, Data curation, Conceptualization.

Declaration of Competing Interest

The authors declare that they have no known competing financial interests or personal relationships that could have appeared to influence the work reported in this paper.

Acknowledgements

TDR gratefully acknowledges financial support received from the UGC-DAE CSR Mumbai Centre under the Collaborative Research Scheme (CRS-M-313), and DST-SERB, India, through the SERB-SURE program [SUR/2022/004508]. This work was supported in part by the U.S. Department of Energy, Office of Basic Energy Sciences under Award No. DE-SC0021973.

Data availability

Data will be made available on request.

References

- [1] S.N. Achary, S.J. Patwe, M.D. Mathews, A.K. Tyagi, Mater. Chem. Phys. 98 (2006) 486–493.
- [2] S. Vasala, M. Karppinen, Prog. Solid State Chem. 43 (2015) 1-36.
- [3] D.K. Mahato, T.P.Sinha, J. Mater. Sci. Mater. Electron. 46 (1) (2016) 107-115.

- [4] Maria Retuerto Man-RongLi, Zheng Deng, Peter W. Stephens, Mark Croft, Qingzhen Huang, Hui Wu, Xiaoyu Deng, Gabriel Kotliar, Javier SánchezBenítez, Joke Hadermann, David Walker, Martha Greenblatt, Angew. Chem. Int. Ed. 54 (2015) 12069–12073.
- [5] Yuichi Shimakawa, Masaki Azuma, Noriya Ichikawa, Materials 4 (2011) 153-168.
- [6] H.L. Feng, Peter Adler, Manfred Reehuis, Walter Schnelle, Philip Pattison, Andreas Hoser, Claudia Felser, Martin Jansen, Chem. Mater. 29 (2017) 886–895.
- [7] N.S. Rogado, J. Li, A.W. Sleight, M.A. Subramanian, M, Adv. Mater. 17 (2005) 2225–2227.
- [8] S. Bhattacharjee, R.K. Parida, B.N. Parida, Mater. Sci. Eng. B 271 (2021) 115234.
- [9] M. Cerne, F. Vasiliu, C. Bartha, C. Plapcianu, I. Mercioniu, Ceram. Int. 40 (2014) 11601–11609.
- [10] W.Chen Witczak-Krempa, G. Kim, Y.B. Balents, L. Annu, Rev. Condens. Matter Phys. 5 (2014) 57–82.
- [11] L.T. Corredor, G. Aslan-Cansever, M. Sturza, Kaustuv Manna, A. Maljuk, S. Gass, T. Dey, A.U.B. Wolter, Olga Kataeva, A. Zimmermann, M. Geyer, C.G.F. Blum, S. Wurmehl, B. Buchner, Phys. Rev. B 95 (2017) 064418.
- [12] P. Kayser, et al., Acta Mater. 207 (2021) 116684.
- [13] (a) S. Sharma, C. Ritter, D.T. Adroja, G.B. Stenning, A. Sundaresan, S. Langridge, Phys. Rev. Mater. 6 (2022) 014407;
 - (b) J. Wang, K. Li, B. Yu, Z. Wu, Comput. Mater. Sci. 60 (2012) 149–152.
- [14] T.Durga Rao, S. Marik, D. Singh, R.P. Singh 705 (2017) 849-852.
- [15] G. Bhavani, T.Durga Rao, Manish K. Niranjan, K. Ramesh Kumar, B. Sattibabu, V. Petkov, E.S. Kannan, B.H. Reddy, Phys. B 695 (2024) 416477.
- [16] W. Kohn, L.J. Sham, Phys. Rev. 140 (1965) A1133.
- [17] G. Kresse, J. Furthmuller, Phys. Rev. B 54 (1996) 11169.
- [18] P.E. Blochl, Phys. Rev. B 50 (1994) 17953.
- [19] J.P. Perdew, K. Burke, M. Ernzerhof, Phys. Rev. Lett. 77 (1996) 3865.
- [20] J. Sun, A. Ruzsinszky, J.P. Perdew, Phys. Rev. Lett. 115 (2015) 036402.
- [21] S.L. Dudarev Dudarev, S.L. Botton, G.A. Savrasov, S.Y. Humphreys, C.J. Sutton, Phys. Rev. B 57 (1998) 1505.
- [22] M. Gajdoš, K. Hummer, G. Kresse, J. Furthmüller, F. Bechstedt, Phys. Rev. B 73 (2006) 045112.
- [23] A. Alsabah, Mohamad S. AlSalhi, Eltayeb M. Mustafa, Abdelrahman A. Elbadawi, Sandhanasamy Devanesan, Mohamed A. Siddig, Mohamed A. Siddig, Crystals 2020 10 (4) (2020) 299.
- [24] V.J. Angadi, K. Manjunatha, K. Praveena, V.K. Pattare, B.J. Fernandesf, S. O. Manjunatha, J. Husain, S.V. Angadi, L.D. Horakeri, K.P. Ramesh, J. Magn. Magn. Mater. 529 (2021) 167899.
- [25] C. Ragupathi, S. Narayanan, P. Tamizhdurai, T.A. Sukantha, G. Ramalingam, M. P. Pachamuthu, V.L. Mangesh, Nadavala Siva Kumar, A.S. Al-Fatesh, S.O. Kasim, Helivon 9 (2023) e21981.
- [26] Md.S. Hossain, Md.A.A. Shaikh, Md.S. Rahaman, S. Ahmed, Mol. Syst. Des. Eng. 7 (2022) 1239.
- [27] S. Yousefi, B. Ghasemi, M.P. Nikolova, J. Cluster Sci. (2021) 1–11.
- [28] Alyea Sofea Kamarulzaman Nor Diyana Abdul Aziz, Zakiah Mohamed Norazila Ibrahim. Materials 15 (2022) 5123.
- [29] (a) G. Blasse, A.F. Corsmit, J. Solid, State chem 6 (1973) 513–518;
 (b) J. M.Gateshki, M. Igartua, E. Hernández-Bocanegra, J. Phys. Condens. Matter 15 (2003) 6199–6217.
- [30] M.Z.M. Halizan, Z. Mohamed, A.K. Yahya, AIP Conf. Proc. 1 (2021) 030005.
- [31] Mebark Elhamel, Zoulikha Hebboul, Djamal Benbertal, Pablo Botella, Daniel Errandonea, Nanomaterials 14 (2024) 960.
- [32] V.M. Gaikward, K.K. Yadav, S.E. Lofland, K.V. Ramanujadrary, S. Chakraverty, A. K. Ganguli, M. Jha, J. Magn, Magn. Mater. 471 (2019) 8.
- [33] C. Li, B. Liu, Y. He, C. Lv, H. He, Y. Xu, J. Alloy. Compd. 590 (2014) 541.
- [34] Yousif A. Alsabah, Abdelrahman A. Elbadawi, Eltayeb M. Mustafa, Mohamed A. Siddig 4 (2016) 61–70.
- [35] J. Ahmad, M. Siddique, J.A. Khan, S.H. Bukhari, T. Sultan, Mater. Res. Express 6 (2019) 126311.
- [36] J.B. Goodenough, A. Wold, R.J. Arnott, N. Menyuk, Phys. Rev. 124 (1961) 373.
- [37] J. Krishna Murthy, K.D. Chandrasekhar, H.C. Wu, H.D. Yang, J.Y. Lin, A. Venimadhav, J. Phys. Condens. Matter 28 (2016).
- [38] T. Ferreira, G. Morrison, J. Yeon, H.C.Z. Loye, Cryst. Growth Des. 16 (2016)
- [39] M. Balli, S. Mansouri, P. Fournier, S. Jandl, K.D. Truong, S. Khadechi-Haj Khlifa, P. de Rango, D. Fruchart, A. Kedous-Lebouc, J. Phys. D Appl. Phys. 53 (2020) 095001.
- [40] A.K. Singh, S. Chauhan, S.K. Srivastava, R. Chandra, Solid State Commun. 242 (2016) 74–78.
- [41] Zhipeng Pei, Kai Leng, Weiren Xia, Yao Lu, Heng Wu, Xinhua Zhu, J. Mag. Mag. Mater. 508 (2020) 166891.
- [42] Shalu Kaushik, Pawan Sharma, Meenal Chauhan, Pooja Sharma, Amit Kumar, Sujata Sanghi, Ashish Agarwal, Mater. Sci. Eng. B 313 (2025) 117965.
- [43] J. Tauc, R. Grigorovici, A. Vancu, Phys. Status Solidi B 15 (1966) 627–637.
- [44] M.Z.M. Halizan, Z. Mohamed, A.K. Yahya, Mater. Res. Express 7 (8) (2020).
- [45] A.H. Slavney, T. Hu, A.M. Lindenberg, H.I. Karunadasa, J. Am. Chem. Soc. 138 (2016) 2138–2141.
- [46] F.N. Sayed, S.N.Deshpande Achary, S.K. Rajeswari, B. Kadam, R.M. Dwebedi, S. Nigam, A.K. Tyagi, A.K.Z. Anorg, Allg. Chem. 640 (2014) 1907–1921.
- [47] Surinder Singh, Anumeet Kaur, Parwinder Kaur, Lakhwant Singh, ACS Omega 8 (2023) 25623–25638.
- [48] Razia Nongjai, Shakeel Khan, K. Asokan, Hilal Ahmed, Imran Khan, J. Appl. Phys. 112 (2012) 084321.
- [49] Z.Ž. Lazarević, Č. Jovalekić, D.L. Sekulić, A. Milutinović, S. Baloš, M. Slankamenac, N.Ž. Romčević, Mater. Res. Bull. 48 (10) (2013) 4368–4378.

- [50] R. Nongjai, S. Khan, K. Asokan, H. Ahmed, I. Khan, J. Appl. Phys. 112 (8) (2012).
- [51] Ilyas Noor Bhattia, Imtiaz Noor Bhatti, Phys. B Phys. Cond. Matter 610 (2021)
- [52] T.Durga Rao, Saket Asthana, Mater. Res. Express 4 (2017) 126305.
 [53] S. Bhagat, K. Prasad, Phys. Status Solidi A 207 (5) (2010) 1232–1239.
- [54] K. Prasad, C.K. Suman, R.N.P. Choudhary, Adv. Appl. Ceram. 105 (2006) 258.
- [55] F.A. Kroger, H.J. Vink, SolidState Phys. 3 (1956) 307.
- [56] M.K. Niranjan, B.R. Sahu, Leonard Kleinman, Phys. Rev. B 70 (2004) 180406.
 [57] Volker L. Deringer, Andrei L. Tchougreeff, Richard Dronskowski, J. Phys. Chem. A 115 (2011) 5461–5466.
- [58] W. Tang, E. Sanville, G. Henkelman, J. Phys. Condens. Matter 21 (2009) 084204.